Supporting Information

Enhancing the Long-Term Photoelectrochemical Performance of TiO_2/Si Photocathodes by Coating of Ti-Doped Mesoporous Hematite

Feng Li[a], Wangshu Zheng[a], Jing Liu*[, a], Liping Zhao[a], Djordje Janackovic[b], Yu Qiu[c], Xuefeng Song[a], Peng Zhang*[, a], Lian Gao[a]

[a] School of Materials Science and Engineering, Shanghai Jiao Tong University, 800 Dongchuan Road, Shanghai 200240, China

[b] Nanotechnology and Functional Materials Centre, University of Belgrade, Karnegijeva 4, Belgrade11000, Serbia

[c] College of Electronics and Information Science, Fujian Jiangxia University, No. 2 Xiyuangong Road, University Town, Fuzhou, Fujian 350108, China

*Corresponding authors: liujing2014@sjtu.edu.cn, pengzhang2010@sjtu.edu.cn

Keywords: photoelectrocatalysis, Si photocathode, long-term stability, Ti-doped hematite, corrosion resistance

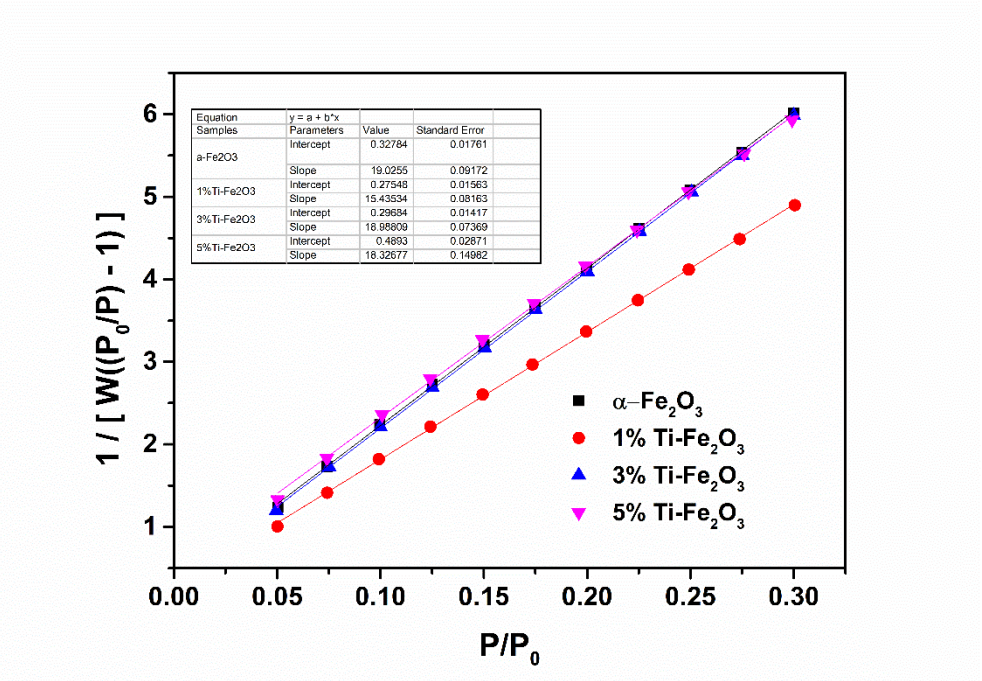

Figure S1. Linear BET plots of 1/[W(P0/P)–1] vs. P/P0 for each sample.

The BET specific surface areas (S) are calculated from the isotherms in the P/P0 range of 0.05 to 0.30 using the Brunauer-Emmett-Teller (BET) equation:

$$\frac{1}{W[\left(\frac{P_0}{P}\right)-1]} = \frac{1}{W_m C} + \frac{C-1}{W_m C}\left(\frac{P}{P_0}\right)$$

$$S = \frac{W_m N A_{cs}}{M}$$

where, W is the weight of gas adsorbed at a relative pressure, P/P0, and Wm is the weight of adsorbate constituting a monolayer of surface coverage. The BET C constant, is related to the energy of adsorption in the first adsorbed layer and consequently its value is an indication of the magnitude of the adsorbent/adsorbate interactions. N is Avogadro's number and M is the molar mass of nitrogen. ACS is the cross-sectional area for nitrogen, which is 16.2 Å^2.

Figure S1 shows linear BET plots of 1/[W(P0/P)–1] vs. P/P0 for each sample. The weight of a monolayer of adsorbate Wm and C can be obtained from the slope b and intercept a of the BET plot. The calculated results are shown in Table S1.

Table S1. A summary on fitting parameters and results for linear BET plots.

Sample	Slope	Intercept	Correlation coefficient, r	C constant	BET specific surface area (m^2/g)
α-Fe_2O_3	19.026	0.3278	0.9999	59.036	180
1%Ti- Fe_2O_3	15.435	0.2755	0.9999	57.024	222
3%Ti- Fe_2O_3	18.988	0.2968	0.9999	64.968	181
5%Ti- Fe_2O_3	18.327	0.4893	0.9997	38.454	185

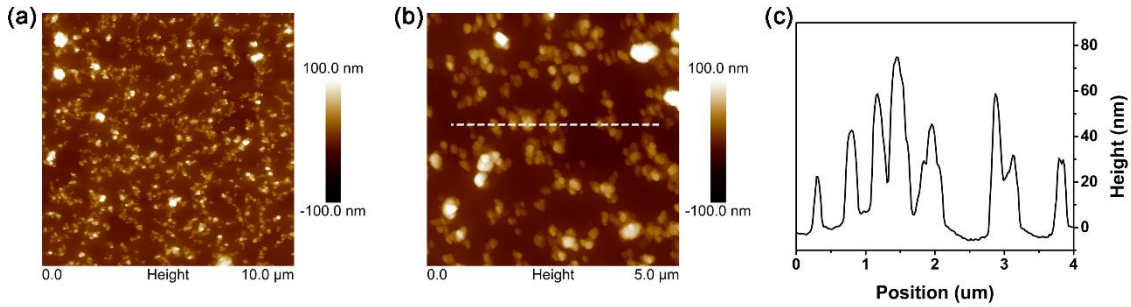

Figure S2. (a-b) AFM images of 3% Ti- Fe_2O_3/TiO2/Si. (c) Height profile derives from the line scan of (b).

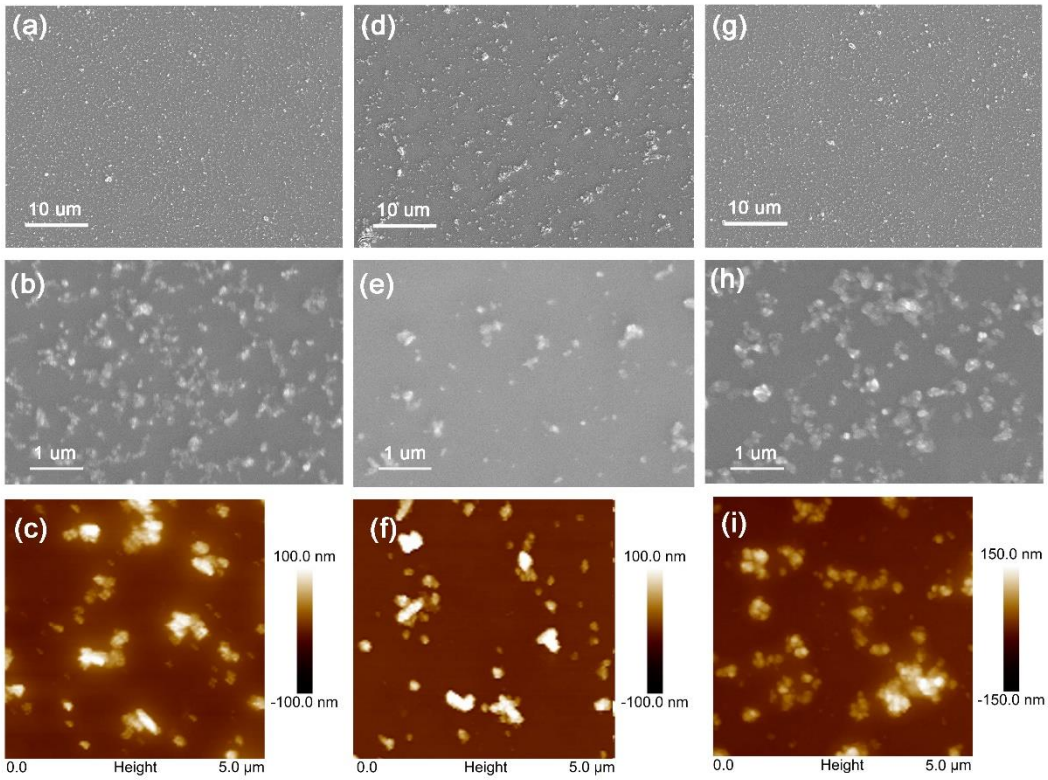

Figure S3. SEM images (a-b) α-Fe_2O_3/TiO_2/Si, (d-e) 1% Ti-Fe_2O_3/TiO_2/Si, and (g-h) 5% Ti-Fe_2O_3/TiO_2/Si. AFM images of (c) α-Fe_2O_3/TiO_2/Si, (f) 1% Ti-Fe_2O_3/TiO_2/Si, and (i) 5% Ti-Fe_2O_3/TiO_2/Si.

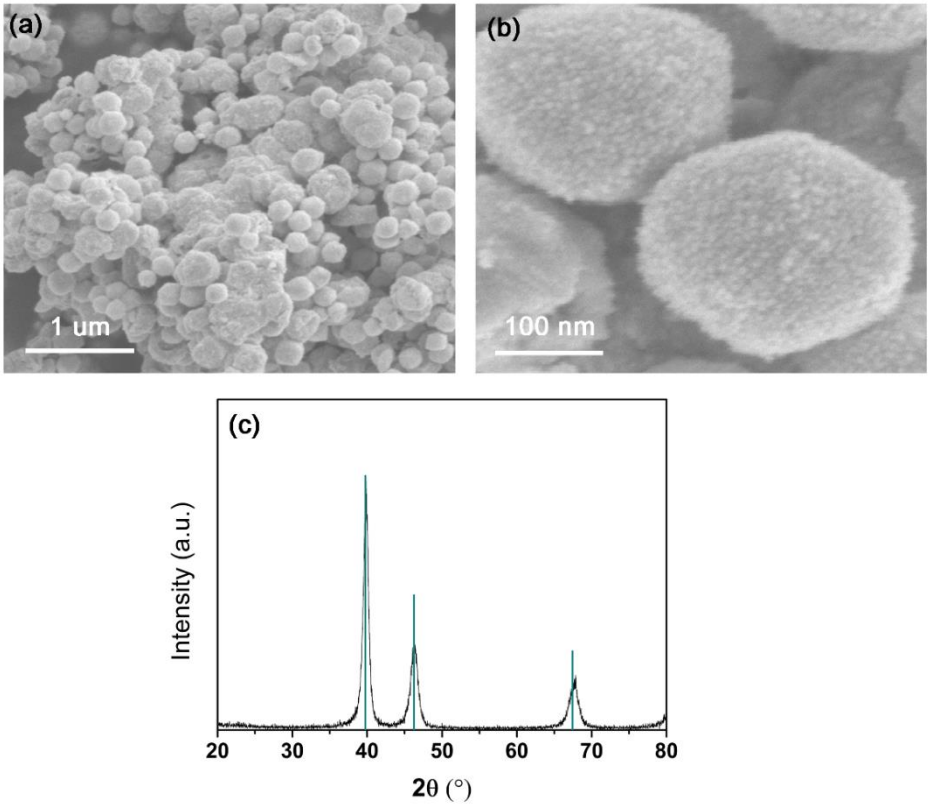

Figure S4. (a-b) SEM images of mesoporous Pt. (c) XRD pattern of mesoporous Pt.

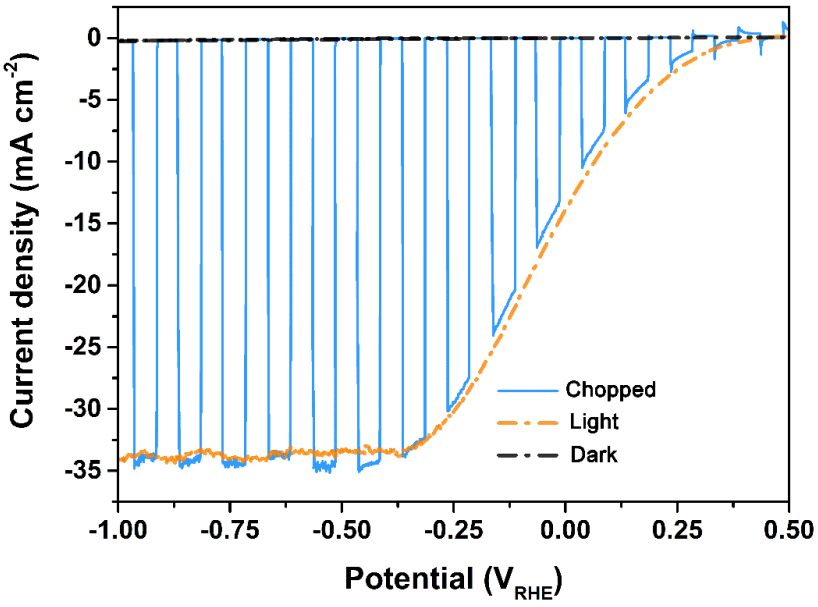

Figure S5. *I-V* curves of 3% Ti-Fe_2O_3/TiO_2/Si in dark, under illumination, and under chopped light.

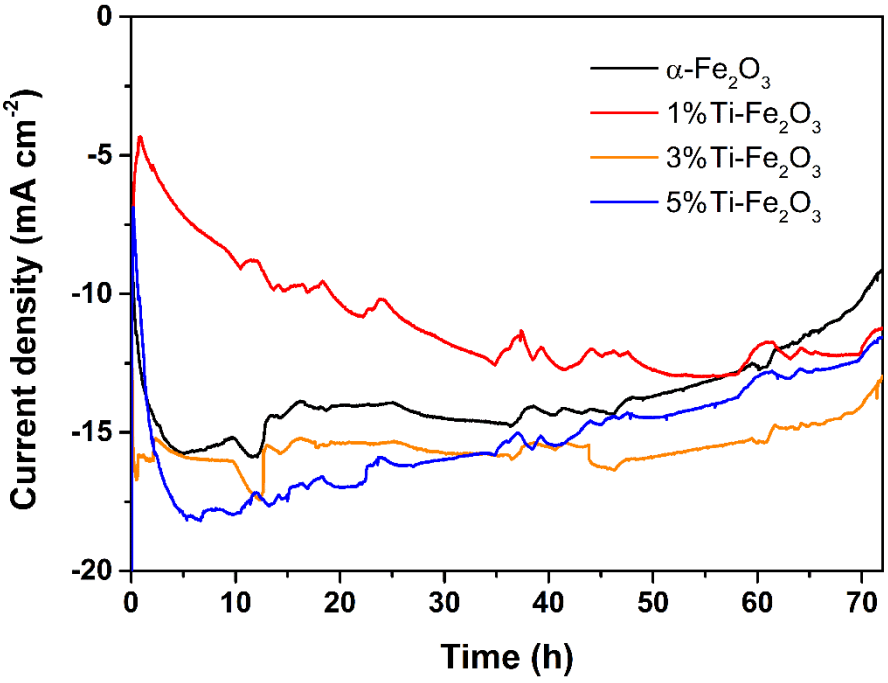

Figure S6. Electrochemical HER stability of α-Fe_2O_3, 1% Ti-Fe_2O_3, 3% Ti-Fe_2O_3, and 5% Ti-Fe_2O_3 at -0.3 V_{RHE} in 1.0 M KOH. The powders were coated on carbon paper with the adhesion of nafion solution.

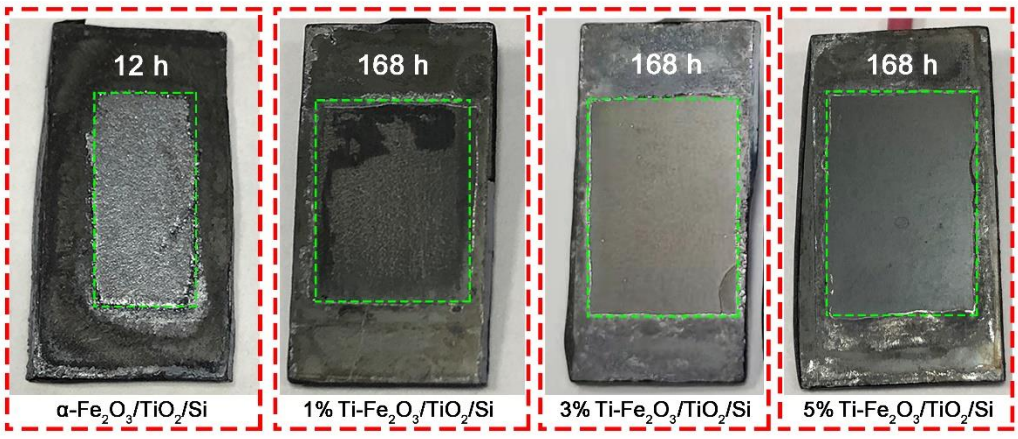

Figure S7. Optical photographs of the α-Fe_2O_3/TiO_2/Si and Ti-Fe_2O_3/TiO_2/Si after stability test, respectively. The regions of green boxes are the test areas.

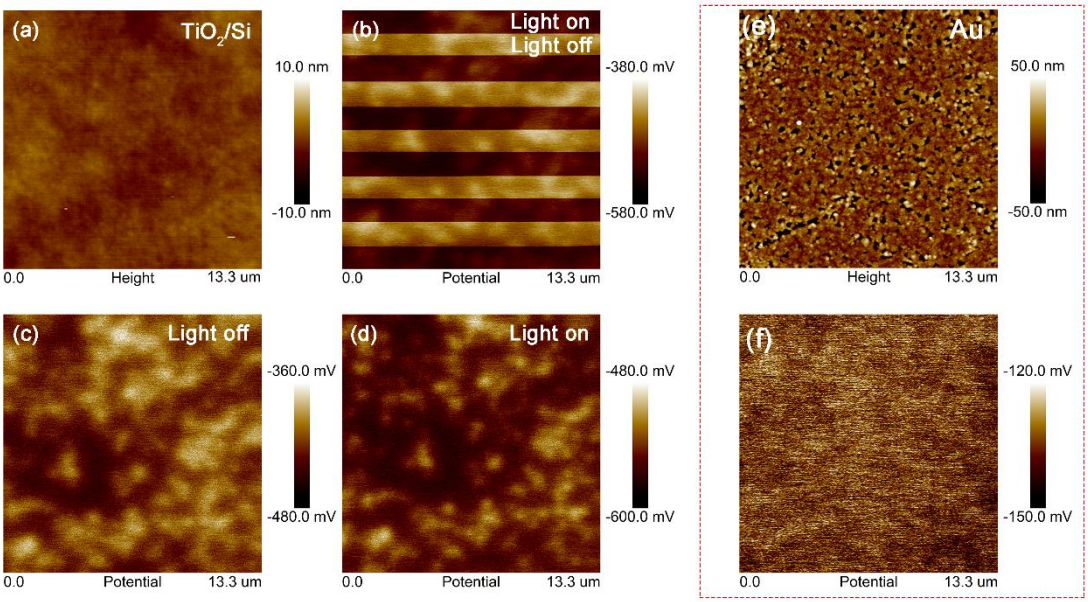

Figure S8. (a-d) AFM image and the corresponding V_{CPD} of TiO_2/Si. (e-f) AFM image and the corresponding V_{CPD} mapping of Au film.

Table S2. A survey on the PEC performance based on Si from recent literature.

Photocathode	Substrate	Electrolyte	Onset potential (V_{RHE})	j (mA cm^{-2}) (0 V_{RHE})	Stability (h)	Ref.
3%Ti-Fe_2O_3/TiO_2/Si	p-Si	1.0 M KOH	0.33 (-1 mA cm-2)	-13.9	168	This work
1%Ti-Fe_2O_3/TiO_2/Si			0.23 (-1 mA cm-2)	-5.1	168	
5%Ti-Fe_2O_3/TiO_2/Si			0.21 (-1 mA cm-2)	-9.4	168	
α-Fe_2O_3/TiO_2/Si			0.24 (-1 mA cm-2)	-5.1	12	
Pt/TiO_2/Si			0.39 (-1 mA cm-2)	-11	38	
Pd/TiO_2/Si	Porous p-Si	1.0 M KOH	0.32 (-0.5 mA cm-2)	-8.3	100	S1
Si/C/TiO_2/Ni-Mo	p-Si MP array	1.0 M KOH	0.36 (-0.5 mA cm-2)	-18	2	S2
Si/TiO_2/MoS_2	Pyramid- shape Si	0.5 M H_2SO_4	0.42 (-0.1 mA cm-2)	-0.24	8	S3
TiO_2/$NiMoO_{4-x}S_x$/TiO_2/Si	p-Si	0.1 M NaH_2PO_4	0.3 (-0.1 mA cm-2)	-0.5	<1	S4
a-Si/Fh/Ni	p-i-n a-Si	1.0 M KOH	0.67 (-0.1 mA cm-2)	-15.6	2.9	S5
p-Si–TiO_2–MoS_2/Rh–P	p-Si	0.5 M H_2SO_4	0.43 (-0.1 mA cm-2)	-24.1	1	S6
PO-MoWS/2 nm TiO_2/Si	p-Si micropyramids	0.5 M H_2SO_4	0.215(-1 mA cm-2)	-11.5	2.2	S7
Pt/Gr/pyramid Si	pyramid Si	1 M $HClO_4$	0.41(-0.1 mA cm-2)	-32.5	30	S8
WP/TiO_2/Si	p-Si	1.0 M KOH	0.27 (-1 mA cm-2)	-15	110	S9
C/α-Fe_2O_3/Si NW	Si nanowires	1 M Na_2SO_4	−0.18(-0.1 mA cm-2)	~0	2	S10

Reference

S1. Zheng, J.; Lyu, Y.; Wang, R.; Xie, C.; Zhou, H.; Jiang, S. P.; Wang, S., Crystalline TiO_2 Protective Layer with Graded Oxygen Defects for Efficient and Stable Silicon-Based Photocathode. *Nature Communications* **2018,** *9* (1), 3572.

S2. Sun, X.; Jiang, J.; Yang, Y.; Shan, Y.; Gong, L.; Wang, M., Enhancing the Performance of Si-Based Photocathodes for Solar Hydrogen Production in Alkaline Solution by Facilely Intercalating a Sandwich N-Doped Carbon Nanolayer to the Interface of Si and TiO_2. *ACS Applied Materials & Interfaces* **2019,** *11* (21), 19132-19140.

S3. Li, X.; Li, Y.; Wang, H.; Miao, H.; Zhu, H.; Liu, X.; Lin, H.; Shi, G., Fabrication of a Three-Dimensional Bionic Si/TiO_2/MoS_2 Photoelectrode for Efficient Solar Water Splitting. *ACS Applied Energy Materials* **2020,** *4* (1), 730-736.

S4. Wu, F.; Tian, W.; Cao, F.; Meng, L.; Li, L., Loading Amorphous $NiMoO_{4-x}S_x$

Nanosheet Cocatalyst to Improve Performance of p-Silicon Wafer Photocathode. *ACS Applied Energy Materials* **2018,** *1* (3), 1286-1293.
S5. Zhang, D.; Du, M.; Wang, P.; Wang, H.; Shi, W.; Gao, Y.; Karuturi, S.; Catchpole, K.; Zhang, J.; Fan, F.; Shi, J.; Liu, S., Hole-Storage Enhanced a-Si Photocathodes for Efficient Hydrogen Production. *Angewandte Chemie-International Edition* **2021,** *60* (21), 11966-11972.
S6. Chen, Z.; Li, Y.; Wang, L.; Bu, Y.; Ao, J.-P., Development of a Bi-Compound Heterogeneous Cocatalyst Modified p-Si Photocathode for Boosting the Photoelectrochemical Water Splitting Performance. *Journal of Materials Chemistry A* **2021,** *9* (14), 9157-9164.
S7. Pichaimuthu, K.; Chen, C. J.; Chen, C. H.; Chen, Y. T.; Su, C.; Wei, D. H.; Liu, R. S., Boosting Solar Hydrogen Production of Molybdenum Tungsten Sulfide-Modified Si Micropyramids by Introducing Phosphate. *ACS Applied Materials & Interfaces* **2020,** *12* (37), 41515-41526.
S8. Ku, C. K.; Wu, P. H.; Chung, C. C.; Chen, C. C.; Tsai, K. J.; Chen, H. M.; Chang, Y. C.; Chuang, C. H.; Wei, C. Y.; Wen, C. Y.; Lin, T. Y.; Chen, H. L.; Wang, Y. S.; Lee, Z. Y.; Chang, J. R.; Luo, C. W.; Wang, D. Y.; Hwang, B. J.; Chen, C. W., Creation of 3D Textured Graphene/Si Schottky Junction Photocathode for Enhanced Photo-Electrochemical Efficiency and Stability. *Advanced Energy Materials* **2019,** *9* (29), 1901022.
S9. Li, F.; Yuan, Y.; Feng, X.; Liu, J.; Chen, S.; Lin, Y.; Sun, Y.; Chen, H.; Zhao, L.; Song, X.; Zhang, P.; Gao, L., Coating of Phosphide Catalysts on p-Silicon by a Necking Strategy for Improved Photoelectrochemical Characteristics in Alkaline Media. *ACS Applied Materials & Interfaces* **2021,** *13* (17), 20185-20193.
S10. Qu, Y.; Li, F.; Zhang, P.; Zhao, L.; Liu, J.; Song, X.; Gao, L., Enhanced Photoelectrochemical Performance and Stability of Si Nanowire Photocathode with Deposition of Hematite and Carbon. *Applied Surface Science* **2019,** *471*, 528-536.